JOURNAL OF APPLIED ELECTROCHEMISTRY 22 (1992) 478–482

Electroless nickel hydroxide: synthesis and characterization

P. VISHNU KAMATH

Department of Chemistry, Central College, Bangalore University, Bangalore-560 001, India

G. N. SUBBANNA

Materials Research Centre, Indian Institute of Science, Bangalore-560 012, India

Received 18 September 1991

An electroless method of nickel hydroxide synthesis through the complexation–precipitation route which yields a fine particle material having a specific surface area of 178 $m^2 g^{-1}$ has been described. The morphology of this material as revealed by electron microscopy is distinctly different from the turbostratic nature of electrosynthesized nickel hydroxide. While the long range structure as shown by the X-ray diffraction pattern is similar to that of β-$Ni(OH)_2$, the short range structure as revealed by infrared spectroscopy incorporates characteristics similar to that of α-$Ni(OH)_2$. Cyclic voltammetry studies show that the electroless nickel hydroxide has a higher coulombic efficiency (> 90%), a more anodic reversible potential and a higher degree of reversibility compared to the electrosynthesized nickel hydroxide and conventionally prepared nickel hydroxide.

1. Introduction

Nickel hydroxide has been a subject of many exhaustive studies [1, 2] because of its application as an electrode material in nickel–cadmium batteries. On account of its commercial importance several methods of nickel hydroxide synthesis have been developed. Merlin's preparation [3] and the method of Fievet and Figlarz [4] leads to the formation of β-$Ni(OH)_2$ while the method of LeBihan and others [5] yields a highly disordered hydrated form of nickel hydroxide designated as turbostratic $Ni(OH)_2$. Electrosynthetically prepared nickel hydroxide [6, 7] has been designated as α-$Ni(OH)_2$. These various forms of nickel hydroxide differ from each other in their crystal structure [8], degree of hydration [9], state of charge [10], short range structure as revealed by infrared spectroscopy [1] and morphology [11]. These differences considerably affect the electrochemical activity of the different forms of nickel hydroxide. It is now generally accepted that electrosynthesized α-$Ni(OH)_2$ has superior electrochemical properties compared to the chemically synthesized β-$Ni(OH)_2$ [1].

While it is difficult to associate superior electrochemical activity of an oxide electrode with any one single determining factor it is nevertheless well known that morphology plays an important part [12–14]. Materials having a high surface area, a high degree of porosity and low particle size have better charge capacity and related indicators of superior electrochemical activity. These considerations prompted us to search for new synthetic approaches to nickel hydroxide and in this paper we report an electroless method of synthesis through the complexation-precipitation route.

The electroless method involves the slow combination of anions and cations homogeneously to yield the product in the form of a thin film or a fine particle material. The kinetics of precipitation is essentially controlled by a complexing agent. This method was first applied to the synthesis of PbO_2 and MnO_2 [15] and later extended to other pure and doped oxides such as In_2O_3 and Sb_2O_3 [16] and NiO [17].

We have extended the electroless method to the preparation of nickel hydroxide and characterized electroless $Ni(OH)_2$ (ELN) by a variety of techniques such as X-ray diffraction (XRD), infrared spectroscopy, BET, electron microscopy and cyclic voltammetry (CV). The properties of ELN have been compared with those of electrochemically synthesized α-$Ni(OH)_2$ (ESN). We report that ELN is a superior electrode material compared to ESN.

2. Experimental details

2.1. *Preparation*

ELN was prepared from a 0.1 M $Ni(NO_3)_2$ solution to which was added trisodium citrate (one equivalent of trisodium citrate per equivalent of Ni^{2+}). KOH (0.1 M) was added in drops with vigorous stirring and the pH was raised to 11.6. The solution remained clear and no precipitation was seen. The clear solution was stored for 12 h when slight turbidity was observed and the pH had come down to 10.5. More KOH was added to make up the pH to 11.3. After a further 6 h of standing a voluminous floating precipitate was seen which did not settle completely even after a week.

The precipitate was filtered slowly through a Whatman 44 filter paper and repeatedly washed with distilled water for over three days until the wash

0021-891X/92

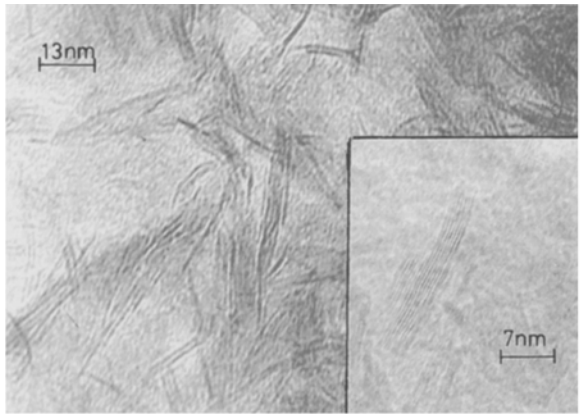

Fig. 1. Transmission electron micrograph of electrosynthesized nickel hydroxide. Inset reveals the lattice fringes observed at high resolution.

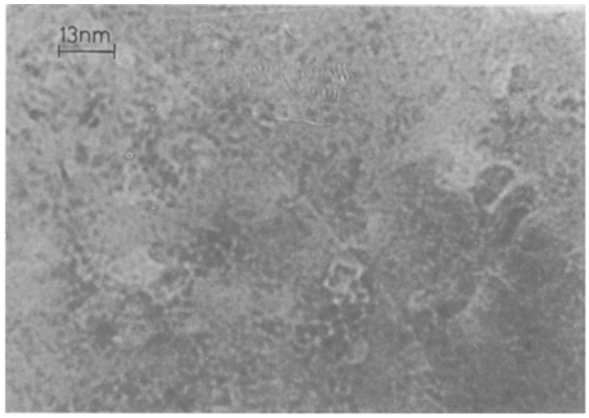

Fig. 2. Transmission electron micrograph of electroless nickel hydroxide.

became neutral. The precipitate was then dried at 55° C to constant weight.

ESN was prepared as described elsewhere [10] by cathodic reduction of the nitrate ion under potentiostatic conditions (− 1.0 V with respect to a SCE) from a 0.2 M $Ni(NO_3)_2$ solution in a divided cell using a platinum flag electrode (1.5 cm^2 surface area). The material was collected from the thick deposits, washed and dried to constant weight at 55° C.

Chemical $Ni(OH)_2$ was prepared by the addition of 0.1 M KOH to 0.1 M $Ni(NO_3)_2$ solution [18] with constant stirring. The green gel-like precipitate settled rapidly. It was filtered and washed with distilled water and dried to constant weight at 55° C.

2.2. *Characterization*

X-ray diffractograms were obtained from a Jeol JDX8P powder diffractometer using Cu$K\alpha$ radiation. Transmission electron microscopic studies were carried out on a Jeol JEM200CX microscope operated at 200 kV. For microscopic observation powder samples were dispersed on holey carbon grids (200 mesh). The surface areas of the samples were measured using a Micrometrics model 2200 particle size analyser. Infrared spectra were recorded on a Perkin Elmer model 580 infrared spectrometer in KBr pellets at a resolution of 3 cm^{-1}.

2.3. *Cyclic voltammetry*

Cyclic voltammetry studies were carried out using a Princeton Applied Research Centre model 362 scanning potentiostat/galvanostat hooked on to a Digital Electronics (India) x–y recorder. A Hg/HgO (1 M KOH) electrode was used as reference and a platinum strip was used as a counter electrode. Freshly prepared 1 M KOH was used as the electrolyte. The working electrode consisted of a platinum flag of 1.5 cm^2 surface area. The electrode was cleaned with detergent and then electrochemically as described elsewhere [19].

A film of ELN was deposited by immersing the clean platinum flag for over 12 h in a solution of $Ni(NO_3)_2$, trisodium citrate and KOH (pH 11.6). Chemical nickel hydroxide was deposited by immersing the clean platinum flag in a $Ni(NO_3)_2$ (0.1 M) solution followed by addition with rapid stirring of KOH (0.1 M). The substrate was allowed to stand for 30 min. ESN was cathodically deposited at a current density of 5 mA cm^{-2} for 5 s.

The nickel hydroxide films were rinsed in distilled water and immersed in a plastic tank containing 30 ml of 1 M KOH. The scan was initiated at 0.0 V. The anodic sweep was carried out upto 0.63 V and the scan reversed. Scans were repeated until the cyclic voltammograms recorded in successive scans were exactly reproducible. Typically each film was scanned

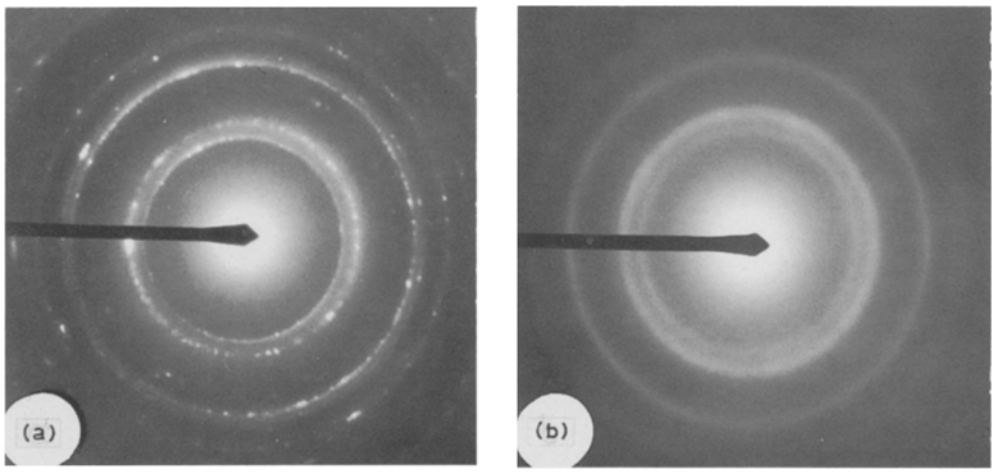

Fig. 3. Electron diffraction patterns of electrosynthesized (a) and electroless (b) nickel hydroxide samples.

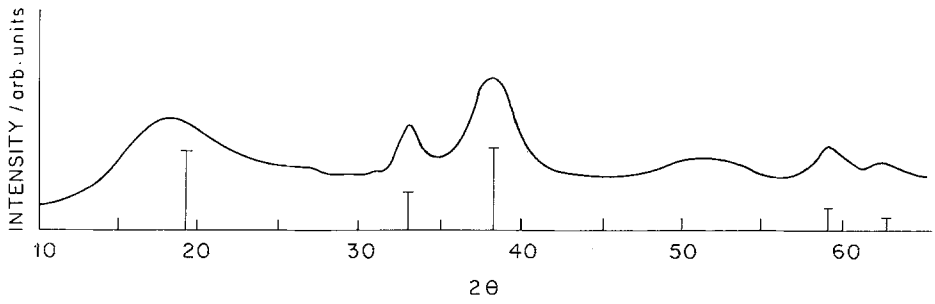

Fig. 4. X-ray diffractogram of electroless nickel hydroxide. The vertical lines show the positions and relative intensities of the lines assigned to β-$Ni(OH)_2$.

through 35 to 40 cycles. Coulombic efficiency was evaluated as the ratio of the cathodic to the anodic peak heights.

3. Results and discussion

3.1. *Morphology and structure*

The most striking feature of ELN is its specific surface area which at $178\,m^2g^{-1}$ is 8 times higher than that of ESN ($20\,m^2g^{-1}$). Typical values observed for other oxide electrode materials vary in the range 5 to $30\,m^2g^{-1}$ [20]. Specific surface area is an important factor determining electrode performance as changes in morphology arising due to the agglomeration of particles is responsible for the diminishing electrode capacity and utilization of electrode material [21] upon cycling. Therefore the observation of high specific surface area in ELN assumes special significance.

The formation of the fine particle material is facilitated by complexation of the Ni^{2+} ions by the citrate ions. This retards the kinetics of precipitation in the pH range 7 to 10. At higher pH, slow homogeneous precipitation occurs which does not permit the agglomeration of particles. The resulting material has very fine particles and a large surface area compared to ESN.

To investigate the reason for this large difference in the surface area the two samples were studied by electron microscopy and the results are given in Figs 1 and 2. It is clear that there is a very fundamental morphological difference between the ESN and ELN samples. The observations on the ESN morphology are in agreement with earlier reports [1] and the turbostratic nature of the particles is evident. The high resolution image reveals the lattice fringes. ELN on the other hand has a completely different morphology and the micrograph shows fine particle aggregates. The electron diffraction patterns of the two samples are shown in Fig. 3. ESN shows sharp ring patterns in keeping with its higher crystallinity while ELN shows a diffuse ring pattern emphasizing its fine particle nature.

To further characterize ELN along the traditional lines of nickel hydroxide polymorphism [8], the X-ray diffractogram of ELN was recorded and is shown in Fig. 4. The peaks are very broad in keeping with the fine particle nature of the material exemplified in the electron micrograph. The pattern matches well with that reported for β-$Ni(OH)_2$ (PDF No. 14-117) except for the slight shift (0.027 nm) to a higher d-value for the (0 0 1) reflection. It may be recalled that the c-axis of nickel hydroxide is highly sensitive to its state of hydration [9] and the higher value observed for ELN is indicative of a greater degree of hydration compared to β-$Ni(OH)_2$.

Any change in the degree of hydration should influence the nature of nickel ion bonding in its first coordination shell. Infrared spectra are very sensitive to these short range structural details and have been used quite effectively [22, 23] in studying hydroxide elec-

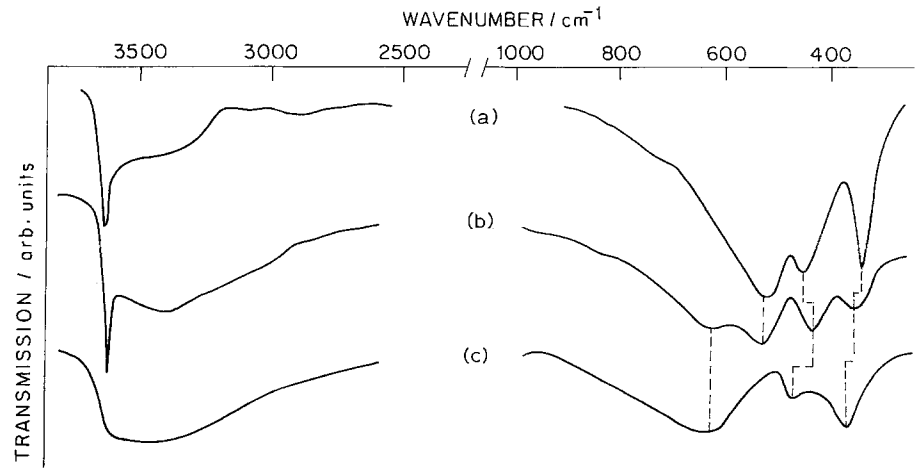

Fig. 5. Infrared spectra of chemical $Ni(OH)_2$ (a) compared with electroless (b) and electrosynthesized (c) nickel hydroxide samples.

Table 1. Structural and morphological properties of electroless $Ni(OH)_2$ compared with α- and β-$Ni(OH)_2$

	Chemical β-$Ni(OH)_2$	*Electroless $Ni(OH)_2$*	*Electrosynthesized α-$Ni(OH)_2$*
Infrared spectra (peak positions in cm^{-1})	3640	3640	3640–3300
	3370(w)	3400	
		630	640
	530	530	
	460	430	470
	345	360	380
Specific surface area ($m^2 g^{-1}$)		178	20
Electron diffraction	Crystalline	Amorphous	Poorly crystalline

trode reactions. Figure 5 shows the infrared spectra of ELN together with the spectra of ESN and conventionally chemically synthesized β-$Ni(OH)_2$. The results are tabulated in Table 1.

In the OH stretching region (3700–3300 cm^{-1}) chemical β-$Ni(OH)_2$ shows a sharp peak in keeping with the characteristic of a highly ordered brucite structure which does not permit hydrogen bonding between the hydroxyl groups [24]. ESN shows a broad band in the 3640–3300 cm^{-1} region indicating a high degree of hydration and consequent extensive hydrogen bonding. ELN shows two distinct features: a sharp peak (3640 cm^{-1}) following by a distinct broad band centred at 3400 cm^{-1} indicating a degree of hydration intermediate between α- and β-$Ni(OH)_2$.

The results at lower frequencies (1000–200 cm^{-1}) are more interesting. Chemically prepared β-$Ni(OH)_2$ shows two strong peaks at 530 and 345 cm^{-1} due to the in-plane and out-of-plane OH deformations respectively and a peak at 460 cm^{-1} due to the Ni–O stretch. In ESN, extensive hydrogen bonding hinders the OH deformations which move to higher frequencies at 640 and 380 cm^{-1}. The Ni–O stretch remains relatively unchanged at 470 cm^{-1}. These results have been reported earlier [1]. ELN shows four bands in this region at 630, 530, 430 and 360 cm^{-1} respectively. This is contrary to expectation from a group theoretical analysis of the brucite type cage which predicts only three bands in this region [25]. One is forced to conclude that ELN has a lattice that admits in-plane deformations of the α (630 cm^{-1}) as well as β (530 cm^{-1}) type. The out of plane deformation at 360 cm^{-1} is intermediate between the α and β type lattices. ELN is however not a mixture of the α and β-$Ni(OH)_2$ phases, as the characteristic lines corresponding to the α-phase cannot be seen in the X-ray diffraction pattern. There is also no evidence for intergrowth structures in the electron micrographs of ELN. As such the exact nature of ELN is not clear.

3.2. *Cyclic voltammetry studies*

Figure 6 shows the cyclic voltammograms of ELN, ESN and chemical $Ni(OH)_2$ samples. All the samples show one anodic and one cathodic peak. The peak potentials due to ELN are significantly different from those of α- and β-$Ni(OH)_2$. The results have been tabulated in Table 2. While α- and β-$Ni(OH)_2$ have similar anodic and cathodic peak potentials, the corresponding potentials of ELN are shifted anodically. The average of the cathodic and anodic potentials which can be taken as an estimate of the reversible potential [19] is 510 mV for ELN compared to 430 to 435 mV for the other two samples. In terms of the cathodic to anodic peak separations, which is a measure of the reversibility [19], ELN has the smallest separation (70–90 mV) compared to ESN (90–100 mV) and chemical $Ni(OH)_2$ (115–125 mV).

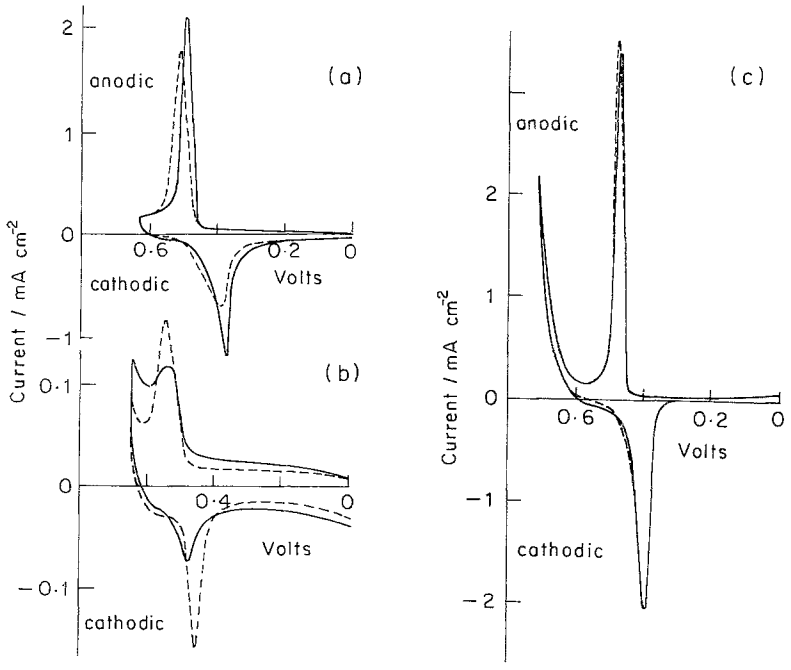

Fig. 6. Cyclic voltammograms of chemical (a), electroless (b), and electrosynthesized (c) nickel hydroxide samples. The full line trace corresponds to the first cycle and dashed line to the 30th cycle.

Table 2. Summary of cyclic voltammetry results\†*

	Anodic peak potential E_a/mV	*Cathodic peak potential* E_c/mV	*Average potential* E_{rev}/mV	*Peak separation* $\Delta E_{a,c}/mV$	*Coulombic efficiency*‡/%
Chemical	490	375	432	115	
β-$Bi(OH)_2$	(510)	(385)	(447)	(125)	35
Electroless	545	475	510	70	
$Ni(OH)_2$	(550)	(460)	(505)	(90)	> 90
Electrosynthesized	480	390	435	90	
α-$Ni(OH)_2$	(490)	(390)	(440)	(100)	61

* All values expressed in millivolts with respect to a Hg/HgO (1^M KOH) reference electrode.
† Figures in parentheses refer to the 30th cycle.
‡ Estimated as ratio of the cathodic to the anodic peak heights in the 30th cycle.

The ratio of the cathodic to anodic peak heights represents the coulombic efficiency of the electrode material. In the ELN case, the two peak heights are nearly equal indicating a better than 90% efficiency while it is 60% for ESN and 35% for chemical $Ni(OH)_2$.

It is thus seen that ELN is a better electrode material than other nickel hydroxide samples prepared by conventional methods. Nickel hydroxide being a high resistivity phase, it is expected that the electrode reactions take place close to the surface of the particles. The reaction interface penetrates into the bulk of the particles by proton diffusion [1] which is by its very nature a slow process. Therefore better utilization of the electrode material will be facilitated by a high specific surface area. ELN's better performance as observed here may be attributed to this.

4. Conclusions

The electroless method of preparation through the complexation–precipitation route is a simple chemical method for preparing a fine particle nickel hydroxide material which shows superior electrochemical properties. The small particle morphology of electroless $Ni(OH)_2$ is completely different from the turbostratic nature of electrosynthesized $Ni(OH)_2$.

References

[1] P. Oliva, J. Leonardi, J. F. Laurent, C. Delmas, J. J. Braconnier, M. Figlarz and F. Fievet, *J. Power Sources* **8** (1982) 229.
[2] R. Barnard, C. F. Randell and F. L. Tye, *J. Appl. Electrochem.* **10** (1980) 61, 109 and 127.
[3] A. Merlin, *C.R. Acad. Sci.* **236** (1953) 1892.
[4] F. Fievet and M. Figlarz, *J. Catalysis* **39** (1975) 350.
[5] S. LeBihan, J. Guenot and M. Figlarz, *C.R. Acad. Sci., Ser. C.* **270** (1970) 2131.
[6] J. A. Switzer, *Am. Ceram. Soc. Bull.* **66** (1987) 1521.
[7] K. C. Ho, *J. Electrochem. Soc.* **134** (1987) 52C.
[8] R. S. McEwen, *J. Phys. Chem.* **75** (1971) 1782.
[9] B. Mani and J. P. de Neufville, *J. Electrochem. Soc.* **135** (1988) 800.
[10] P. V. Kamath and N. Y. Vasanthacharya, *J. Appl. Electrochem.* (1991), in press.
[11] E. J. McHenry, *Electrochem. Technol.* **5** (1967) 275.
[12] S. N. Kanungo, K. M. Parida and B. R. Sant, *Electrochim. Acta* **26** (1981) 1147.
[13] J. B. Fernandes, B. D. Desai and V. N. Kamat-Dalal, *ibid.* **29** (1984) 187.
[14] R. D. Armstrong and E. A. Charles, *J. Power Sources* **25** (1989) 89.
[15] W. Mindt, *J. Electrochem. Soc.* **117** (1970) 615; **118** (1971) 93.
[16] D. Raviendra and J. K. Sharma, *J. Phys. & Chem. Solids* **46** (1985) 945.
[17] P. Pramanik and S. Bhattacharya, *J. Electrochem. Soc.* **137** (1990) 3869.
[18] O. Glenser, 'Handbook of Preparative Inorganic Chemistry', Vol. 2, Academic Press, New York (1965) pp. 1549.
[19] D. A. Corrigan and R. M. Bendert, *J. Electrochem. Soc.* **136** (1989) 723.
[20] K. J. Euler and H. M. Helsa, *J. Power Sources* **4** (1979) 77.
[21] R. D. Armstrong and E. A. Charles, *ibid.* **27** (1989) 15.
[22] P. V. Kamath and S. Ganguly, *Mater. Lett.* **10/11** (1991) 537.
[23] J. Ismail, M. F. Ahmed and P. V. Kamath, *J. Power Sources* **36** (1991) 495.
[24] W. R. Busing and H. A. Levy, *J. Chem. Phys.* **26** (1957) 563.
[25] S. S. Mitra, *Solid State Phys.* (USA) **13** (1962) 1.